Flight Experiment Demonstrating Existence of Re-entry Vehicle Nosetip Transient Shock Waves

J.M. Cassanto,* A. Monfort,† and C. Fehl‡
General Electric Company, Philadelphia, Pa.

A flight experiment to demonstrate the existence of nosetip transient shock waves (oscillating shocks) has been conducted successfully on a re-entry vehicle (R/V) that contained a high-frequency-response pressure sensor. The pressure sensor was a solid-state device located 18% of the R/V length from the nosetip. The nosetip ablated shape was mapped utilizing recession sensors. A wind-tunnel test program was conducted which demonstrated that an oscillating bow shock wave could be detected on the R/V frustum $\sim 18\%L$ from the nosetip with the flight pressure sensor in the flight port geometry. The flight pressure data were maximum in the low-altitude regime, where the nose recession data showed a severe asymmetric nose cusp configuration. Power spectral density plots of the flight test pressure data showed the existence of an oscillating bow shock wave in this altitude regime. The frequency of the oscillating shock detected in flight was found to be in excellent agreement with the ground-test data when plotted as a function of Strouhal number.

Nomenclature

d	= port diameter, in.
D	= shoulder diameter
h	= altitude
F	= oscillating shock frequency
l	= port length
L	= spike length
L/D	= spike length to shoulder finess rates
M_∞	= freestream Mach number
MPS	= miniature pressure sensor
P	= pressure, psi
$\tilde{P}_{\text{rms}}$	= root-mean-square fluctuating pressure
ΔP	= pressure differential ($P_{\max} - P_{\min}$) due to oscillating shock
S_h	= Strouhal number FL/V_∞
T	= time
T_R	= rise time, sec
X/L	= sensor location is percent of vehicle length
V_∞	= freestream velocity

Introduction

NOSETIP transient shocks have been observed[1-3] in wind-tunnel tests on subliming models that simulate the changing ablated shape of an R/V nosetip during re-entry. Figure 1 presents Schlieren photographs of a camphor model in the Naval Ordnance Laboratory (NOL) ground-test facility taken at four discrete times during a typical run illustrating this trend. Photograph 1 shows the unablated sphere cone configuration simulating an R/V nosetip and shows a single bow shock wave. Photograph 2, taken later in the run, shows that the nosetip has started to sharpen up because of nosetip transition, and to assume its ablated shape. Photograph 3 indicates that the model has assumed a slender concave cusp configuration and shows the formation of a secondary embedded shock due to the cusp. This cusp configuration is considered to be the steady-state turbulent shape[4] and remains constant during the remainder of the run. Note that the ablated shape in photograph 4 is essentially identical with the ablated shape in photograph 3; however, both the bow shock and secondary embedded shock can be seen to be markedly different, even though the wind-tunnel conditions and the configuration have remained fixed. This change in the shock system is referred to as a nosetip transient shock or an oscillating bow shock wave.

Later tests[5] in the same facility, also with ablating models, showed similar results – namely that, for a fixed geometry, the bow and secondary shock system due to the cusp ablated shape can produce an unstable bow shock wave system; a nosetip transient shock. Based upon these results, a flight experiment was proposed[6] and approved to assess the existence of an oscillating bow shock on an R/V by measuring the forebody pressure as close to the nose as possible with a high-frequency-response solid-state pressure transducer. In addition, the R/V also utilized nose recession sensors to map the nose shape change history during the flight.

The oscillating shock flight experiment, however, required two basic ground tests to establish flight feasibility: 1) shock-tunnel tests to determine the frequency response of the pressure sensor/port combination; and 2) wind-tunnel tests to

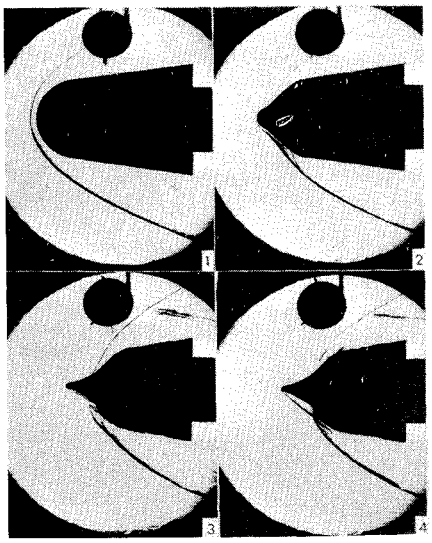

Fig. 1 Ablating model tests showing nosetip transient shock.

Presented as Paper 76-54 at the AIAA 14th Aerospace Sciences Meeting, Washington, D.C., Jan. 26-28, 1976; submitted May 27, 1976; revision received Feb. 14, 1977.

Index categories: LV/M Testing, Flight and Ground; Nonsteady Aeodynamics.

*Project Engineer, Re-entry and Environmental Systems Division. Member AIAA.

†Dynamics Engineer, Re-entry and Environmental Systems Division.

‡Thermodynamics Engineer, Re-entry and Environmental Systems Division.

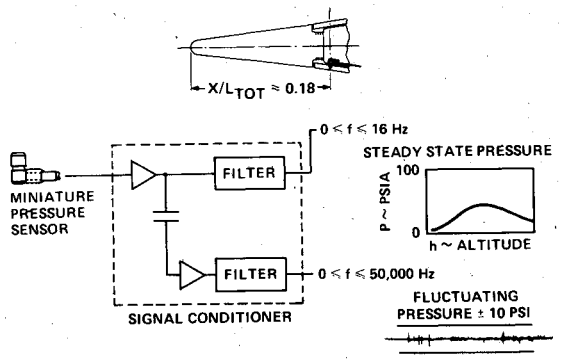

Fig. 2 Dual-band pressure-measurement system for flight experiment.

determine if an oscillating bow shock wave could be detected downstream on the frustum of an R/V, and to determine the magnitude of the oscillating shock pressure measured on the frustum to size the flight signal conditioner. The purpose of this paper is to report on the results of the oscillating shock flight experiment and complimentary ground tests required to establish the feasibility of the flight experiment.

R/V Configuration and Instrumentation

The concept of measuring both steady-state and fluctuating pressures with a solid-state transducer has been proposed[7] for R/V's as a technique to determine both the in-flight pressure distribution (with steady-state pressures) and the onset of boundary-layer transition acoustically (with fluctuating pressures). That concept is now expanded to include oscillating shocks. Figure 2 shows a schematic of the dual-band pressure-measurement system. The R/V telemetry system had the capability to transmit high-frequency-response data with a 25 kHz bandwidth continuous channel.

The nosetip region of the re-entry vehicle that flew the experiment also is shown in Fig. 2. Note that the most forward location available for the pressure transducer is 18%L of the total vehicle length aft of the unablated stagnation point. Details of the pressure port design utilized will be discussed subsequently.

Pressure Transducer

The pressure transducer chosen for this experiment was a solid-state miniature semiconductor strain gage sensor[8] having a four-element active bridge circuit. The strain gage elements are an integral part of the diffused silicon diaphragm. A reference pressure tube permits operation of the transducer as either a differential or absolute sensor. All of the sensors employed in this program were absolute units utilizing a sealed reference pressure. The wind-tunnel sensors had static pressure ranges of 25, 50, and 200 psia, whereas the flight sensor had a range of 0 to 100 psia. Miniaturized solid-state pressure transducers have been under investigation since 1971[9] to obtain a replacement pressure sensor for the conventional potentiometer sensor that has been utilized on re-entry vehicles during the past decade. The main advantage of the solid-state sensor is that it has a high enough frequency response so that it can measure both fluctuating and steady-state pressures. This means that the R/V pressure distribution and, hence, inviscid forebody drag can be obtained from the steady-state measurements, whereas boundary-layer transition onset and the existence of oscillating shocks can be detected by the fluctuating pressure measurements. Another basic advantage of the solid-state sensor is its small size, which allows the sensor to be located in the forward section of an R/V near the nosetip. The flight sensors were temperature-compensated to 250°F and were capable of operating in an environment of 450°F for an extended period of time.

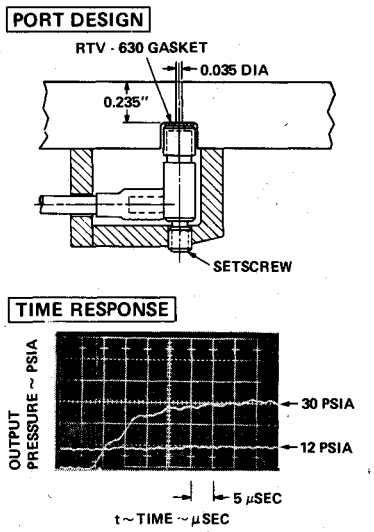

Fig. 3 Rise-time characteristics of solid-state pressure sensor in flight port geometry (shock-tunnel test).

Shock-Tunnel Frequency Response Pressure Sensor Tests

Shock-tunnel tests were conducted to evaluate the effects of pressure port length and diameter on frequency response. The port diameter was fixed in the range between 0.030 and 0.040 in. to minimize pressure port erosion effects.[10] The frequency response for the pressure-measurement system was found to be independent of port passage length. Therefore, the exact flight port geometry was chosen to make the port diameter as large as possible and port length as short as possible (consistent with thermal constraints and erosion requirements) to maximize the frequency response of the pressure port/sensor.

The optimized pressure port flight port geometry ($d=0.035$ in., $l=0.235$ in.) and a flight sensor sans protector demonstrated that the rise time was on the order of 15 μsec (Fig. 3). Calculations from this rise time indicated that the flight pressure port and sensor combination has a frequency response in excess of ~25 kHz (the telemetry bandwidth for the flight experiment). Based on these tests, it was concluded that an acceptable port design had been demonstrated.

Wind-Tunnel Tests

Supporting ground "tests" were conducted in the Naval Ordnance Laboratory (NOL wind Tunnel 8) at a Mach number $M_\infty = 5$ for various Reynolds numbers in turbulent flow.[11] The wind-tunnel model utilized a severe cusp nose shape that had produced an oscillating bow shock wave on previous wind-tunnel tests.[5] Figure 4 shows optical data[5] on the cusp shape illustrating the oscillating bow shock wave phenomena ($F \approx 1300$ cps). A full-scale model of the nosetip and forward frustum was used in the present test with a short- and medium-length nosetip. The model nosetip used in the present test is approximately one-third of the model nosetip size from Ref. 5. This size difference will become important later when it will be shown to affect the frequency of the oscillating shock. The present model was instrumented extensively with quick-response solid-state pressure transducers. One sensor was located on the forward face of the nose cusp to measure the oscillating bow shock frequency and pressure

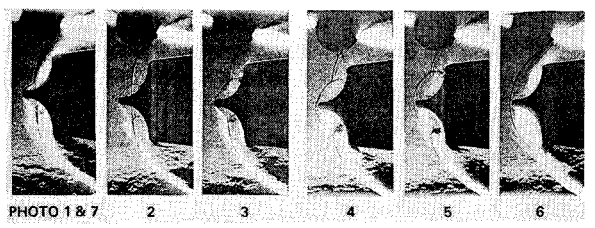

Fig. 4 Test showing oscillating shock (stainless-steel model).

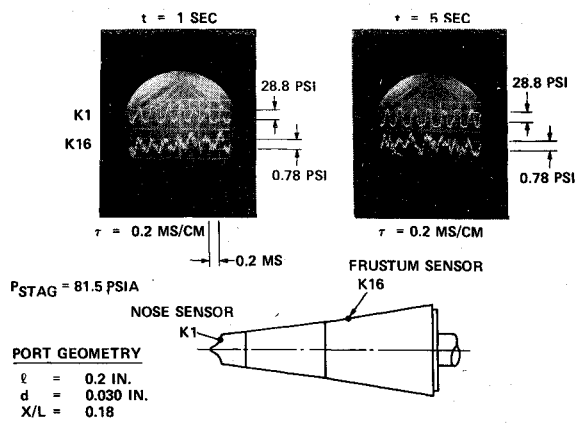

Fig. 5 Oscillating shock pressure data for nose and frustum sensors.

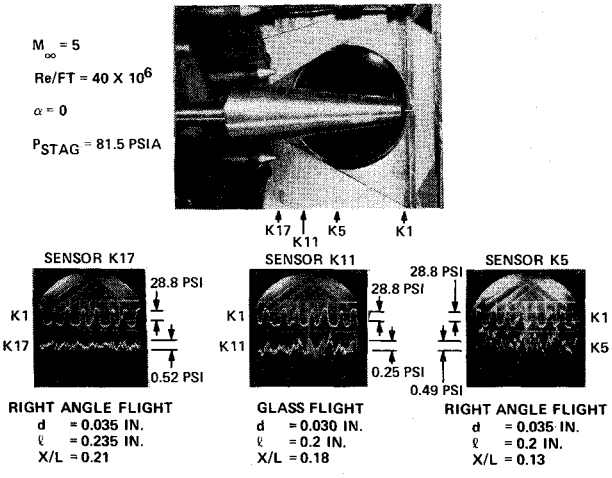

Fig. 6 Oscillating shock wind-tunnel pressure test data compilation.

magnitude. Additional pressure sensors were located along an axial ray forward and aft of the prime flight station to determine the attenuation factor of the oscillating shock pressure. Various pressure sensor port designs were located at the prime flight location on the frustum ($X/L=0.18$). In addition, the exact flight pressure port geometry and two flight pressure sensors were tested.

Pressure data from the high-Reynolds-number run which simulated the flight Reynolds number ($Re/\text{ft}\approx 40\times 10^6$) are shown in Fig. 5 for two times during the run. Several points are significant:

1) The pressure sensor on the nose (K1) shows the effect of the oscillating bow shock wave by responding with an oscillating pressure ($\Delta P\approx 60$ psi) that is the same order of magnitude as the stagnation pressure, $P_{stag}=81.5$ psia. The oscillation frequency of the K1 pressure data is ~ 3000 cps, in good agreement with the optical data.

2) The pressure sensor on the frustum at the prime flight station (K16) clearly senses the oscillating bow shock wave and can be seen to record an oscillating bow shock wave and an oscillating pressure at the same frequency as the nose sensor (K1).

3) The magnitude of the oscillating shock pressure on the frustum is attenuated by approximately two orders of magnitude and has a $\Delta P\approx 0.7$ psi.

The wind-tunnel model and additional pressure data from flight sensors at three axial stations ($X/L=0.13$, 0.18, 0.21) on the frustum are presented in Fig. 6. These data show that the oscillating bow shock wave can be detected on the frustum as far back as 21% of the vehicle length from the stagnation point. It is significant to note that the flight sensors at stations $X/L=0.13$ and 0.18 (K5, K11) were mounted in port

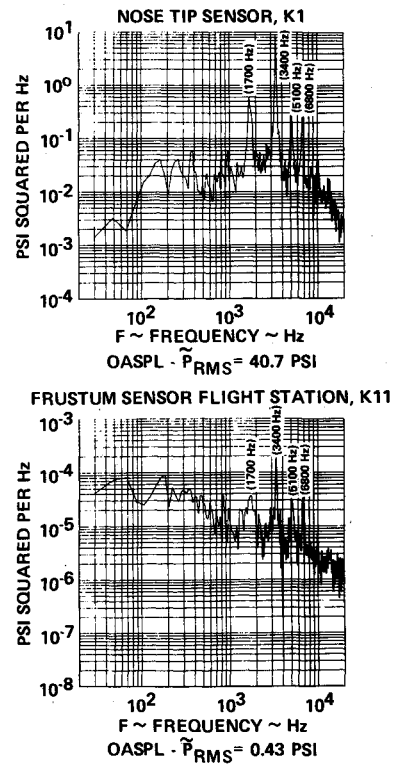

Fig. 7 Oscillating shock ground-test data power spectral density plots.

geometries that approximated the flight geometry. However, sensor K17 ($X/L=0.21$) was a flight sensor in the exact flight port geometry (see Fig. 3). In addition, the flight sensor in K17 was a prime unit that actually was flown on the re-entry vehicle in the flight experiment.

The oscillating pressure differential (ΔP) measured on the frustum from the wind-tunnel test ($\Delta P\sim 0.25$ to 0.75 psi) yielded a range of $\Delta P\sim 5$ to 10 psi when extrapolated to the flight conditions. This magnitude was within the detectable level required for a successful flight experiment. Accordingly, the flight feasibility of the experiment was demonstrated based on the wind-tunnel results.

Power spectral density (PSD) plots of the ground-test pressure data from the nose sensor K1 and a frustum sensor at the flight station are shown in Fig. 7. The prime oscillating shock frequency clearly is seen to be 3400 Hz, in basic agreement with optical data. This oscillating shock frequency is higher than the data of Ref. 5 because the model size is one-third smaller, and oscillating shock frequency scales with model size and Strouhal number. Higher harmonics of the prime oscillating shock frequency also can be seen. The PSD plots for sensors K1 and K11 can be seen to be very similar, with the exception of the level. The $\tilde{P}_{rms}$ for the frustum sensor (K11) can be seen to be two orders of magnitude lower than the nose sensor (K1), as previously discussed.

Oscillating bow shock waves have been studied extensively by Wood[12] and Heyser[13] using test data from cylinders with spikes, and oscillating shock frequency has been correlated as a function of Strouhal number FL/V_∞. It has been suggested[14] that Strouhal number is an effective way to scale oscillating shock frequency from various wind-tunnel tests for different model sizes and velocities to full-scale flight conditions. The Heyser correlation on spiked bodies has been found to predict effectively the oscillating bow shock frequency for the present tests and with previous tests of the severe nose cusp.

Flight Data Results

An oscillograph record of the fluctuating pressure data for low altitudes where significant nosetip ablation and shape change occurs is presented in Fig. 8. Note that there are

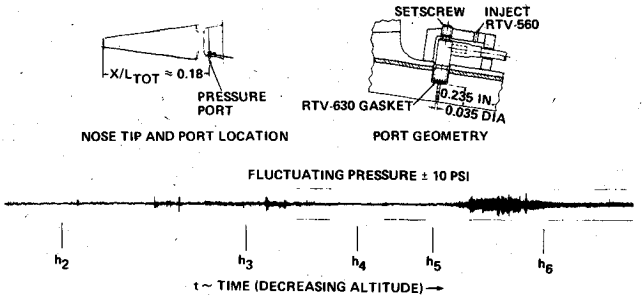

Fig. 8 Flight-test fluctuating pressure data from oscillating shock flight experiment.

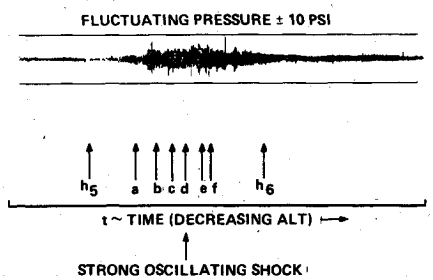

Fig. 9 Fluctuating pressure data during altitude regimes h_5 and h_6.

random "bursts" of data between altitudes h_2 and h_4. PSD plots of the data in this region are broadband and show no significant trends. The ablated shape for altitude h_2 is believed symmetric (a slender cusp) and is based on a single centerline recession data point and the predicted ablated shape.

In addition, ablated shapes derived from the nosetip recession sensors (in the pitch plane) and ablated shapes inferred from motion sensor/windward meridian data (in the yaw plane) shown the beginning of an asymmetric ablated nose shapes for altitudes h_3 and h_4. The ablated shape data for altitude h_4 strongly hint/suggest the existence of the beginning of a severe nose cusp (concave shape) in the pitch plane.

A significant "burst" of large-magnitude fluctuating pressure data exists for 0.4 sec between altitudes h_5 and h_6 (Figs. 8 and 9). The magnitude varies from $\Delta P \sim 4$ psi with spikes to $\Delta P \sim 9.0$ psi. This represents the longest-duration and highest-magnitude fluctuating pressure data obtained during the flight. The nosetip recession sensors for altitude h_5 (just prior to the burst of pressure data) indicate that the ablated shape has developed a severe nose cusp (concavity with a 90° slope), which is conductive to instabilities within the boundary layer and hence an oscillating bow shock wave. The nosetip ablated shape after the "burst" of pressure data (h_6) is more symmetric based on the recession data and has lost the "cusp" configuration."

Power spectral density (PSD) plots were generated in the altitude region during the "burst" of fluctuating pressure data (between h_5 and h_6) to determine the frequency content of the data. The PSD plots are shown in Fig. 10 and were generated for 60-msec time increments between altitudes h_5 and h_6. PSD plots 10a and 10b show a typical broadband response, with the data for frequencies greater than ~12 KHz tending to decay and roll off. This is believed to be due to the port "cutting off" for $f > 12$ kHz. Although step function pressure shock-tunnel ground tests indicated that the design pressure port ($l = 0.235$ in., $d = 0.035$ in.) had a frequency response in excess of the telemetry bandwidth ~25 kHz, the shock-tunnel tests were for a static "no-flow" condition. Hypersonic flow flight conditions apparently tend to increase the rise time and decrease the frequency response. PSD plot 10c shows the beginning of a peak at a frequency of ~12 kHz. PSD plot 10d, taken 60 msec later, clearly shows a distinct

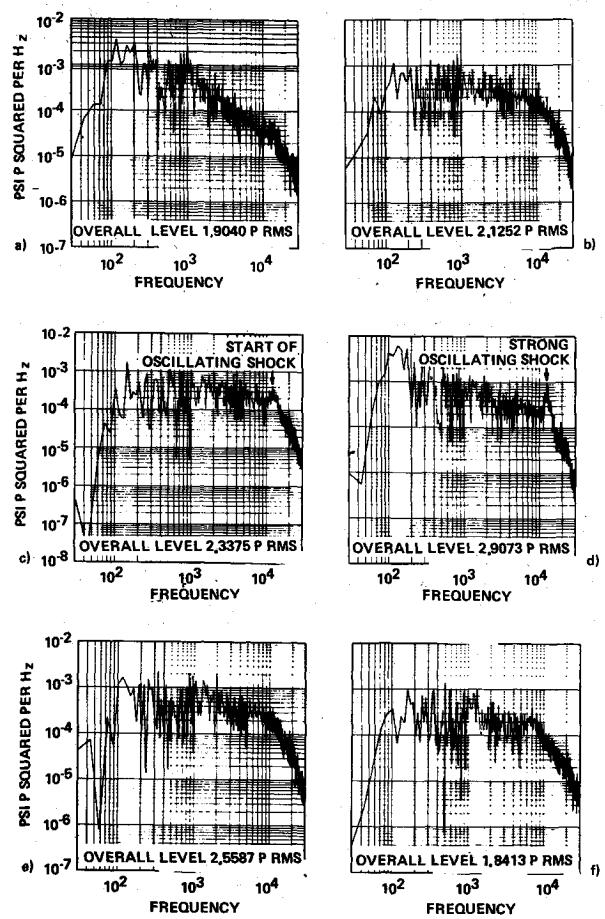

Fig. 10 PSD plots of fluctuating pressure during altitude regimes between h_5 and h_6.

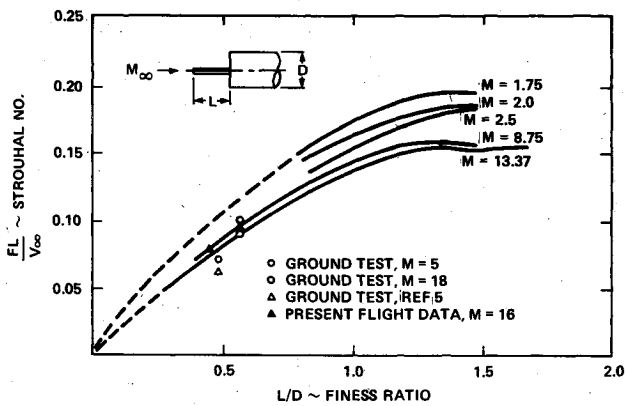

Fig. 11 Oscillating shock Strouhal frequency correlation (flight- and ground-test data).

peak at 12.4 kHz. This peak is indicative of an oscillating bow shock wave. PSD plots 10e and 10f show that the oscillating bow shock wave has disappeared. It is hypothesized that the deep cusp shape (with 90° shoulder) for altitude h_5 produces the oscillating shock for a 100-msec time period, and then the ablated shape changed (based on the recession data) to a slightly blunter nose geometry, which is more stable and not conductive to an oscillating shock.

The flight- and ground-test data from the present experiment have been utilized to update the Heyser correlation. Note that ground tests have been expanded to include $M_\infty = 18$ data, in addition to the flight data. Both the flight- and ground-test oscillating shock frequency data correlate well with Strouhal number is plotted as a function of nosetip L/D ratio (Fig. 11).

Concluding Remarks

A flight experiment has been conducted successfully to determine the existence of a nosetip transient shock on a re-entry vehicle that contained a solid-state high-frequency-response pressure sensor near the nosetip at 18% length. Also included in the flight experiment was nose recession instrumentation to map the ablated nosetip shape. A wind-tunnel test program was conducted at a Mach number of 5 which demonstrated that an oscillating bow shock wave could be detected on the re-entry vehicle frustum 18% of the length from the nosetip with the flight pressure sensor in the flight port geometry. The ground tests also showed that the magnitude of the oscillating shock pressure on the frustum was attenuated by two orders of magnitude from the stagnation oscillating shock pressure. Data from the flight experiment showed that the fluctuating pressure data were maximum in the low-altitude regime where the nose instrumentation showed a severe asymmmetric nose cusp (90° shoulder) configuration. Power spectral density plots of the fluctuating pressure flight data showed the existence of an oscillating bow shock wave in this altitude regime. The frequency of the oscillating shock from the flight experiment was found to be in excellent agreement with the ground-test data when the data were plotted as a function of Strouhal number.

References

[1]Abbett, M.J., "Unsteady Flow on Ablated Nosetip Shapes Pant Series G Test and Analysis Report," Aerotherm Rept. 73-87, Dec. 1973.

[2]Derbidge, T.C., Wood, M.R., and Baker, D.L., "Pant Series D Wind Tunnel Test Data Report," Aerotherm Project 7044, Jan. 1973.

[3]Baltakis, F., "Pant Series C and D Ablation Characteristics Wind Tunnel Test Data," Naval Ordnance Lab. Rept. 68, Jan. 1973.

[4]Brant, D., "Nose Shape Change Code," General Electric Co. RESD TIS (to be published).

[5]Baltakis, F.P., "Pant Series D and E Fluctuating Pressure and Structural Vibration Wind Tunnel Test Data," Naval Ordnance Lab. Rept. 69, Jan. 1973.

[6]Cassanto, J.M., "Oscillating Shock Flight Experiment," General Electric Co., RESD TIS (to be published).

[7]Cassanto, J.M. and Rogers, D.A., "An Experiment to Determine Nose Tip Transition with Fluctuating Pressure Measurements," AIAA Paper 76-625, Bethesda, Md. July 8-10, 1974.

[8]Kicks, J., "Notes on Applications of Integrated Sensor (IS) Pressure Transducer," Kulite Semiconductor Products Inc., Application Note KPS AN11, Dec. 1971.

[9]Cassanto, J.M., Rogers, D.A., Droms, C., and Robison, A., "Use of a Miniature Solid State Pressure Transducer for R/V Flight Test Application," *ISA 20th International Aerospace Instrumentation Conference*, Albuquerque, N. Mex., June 1974; also General Electric Co. RESD TIS 73SD251, Dec., 1973.

[10]Cassanto, J.M., "An Assessment of Pressure Port Erosion Effects," AIAA Paper 75-150, Pasadena, Calif., Jan. 20-22, 1975; also General Electric Co. RESD ALDM 71-108, July 1971.

[11]Fehl, C.J., Monfort, A., and Cassanto, J.M., "Final Analysis of the $M=5$ NOL Wind Tunnel Oscillating Shock Test in Support of the Kulite Flight Experiment," General Electric Co. RESD TDM 9380-003, Sept. 1973.

[12]Wood, C.J., "Hypersonic Flow Over Spiked Cones," *Journal of Fluid Mechanics*, Vol. 12, Dec. 1962, pp. 614-624.

[13]Heyser, A., Wyburny, W., and Kabelitz, H., "Der Stobucllenwindhanal Der DVL – Groundlangen Und Earst Untersuchungen," *Hyperschall – Kolloguuim*, Vom. 14.6, Bis 16.6, St. Louis, June 1966.

[14]Galif, A., "ABRES-NOL-TRW/Wind Tunnel Tests," TRW Rept. Memo. 8523-6-72-83, Dec. 4, 1972.

[15]Maguire, B.L. and Fehl, C., "Experimental Investigation of Ported Pressure Sensor," General Electric Co. RESD Rept. (to be published).

[16]Abbett, M.J. and Cooper, L., "Flow Characteristics About Concave Forebodies at High Mach No.," AIAA Paper 75-153, Pasadena, Calif., Jan. 20-22, 1975.

[17]Baltakis, F., "Wind Tunnel Study of Oscillating Flow Induced Surface Pressures on a Tension-Cone Geometry Model," Naval Ordnance Lab. Rept. 74-134, Jan., 1974.